Optics Letters

Optimization of primary Kerr optical frequency combs for tunable microwave generation

Souleymane Diallo[1] and Yanne K. Chembo[1,2,*]

[1]FEMTO-ST Institute, Université Bourgogne Franche-Comté, CNRS, Optics Department, 15B Avenue des Montboucons, 25030 Besançon cedex, France
[2]GeorgiaTech-CNRS Joint International Laboratory [UMI 2958], Atlanta Mirror Site, School of Electrical and Computer Engineering, 777 Atlantic Dr NW, Atlanta, Georgia 30332, USA
*Corresponding author: yanne.chembo@femto-st.fr

Received 13 June 2017; revised 9 August 2017; accepted 10 August 2017; posted 14 August 2017 (Doc. ID 298036); published 6 September 2017

We analyze the condition under which Kerr combs generate the highest microwave output power after photodetection. These optimal comb states correspond to configurations in which the sidemode-to-pump ratio is the highest possible. For the case of primary combs, we show how the interplay between the power and frequency of the pump laser critically influences this ratio, which has a direct influence on the phase noise performance of the generated microwaves. We also experimentally demonstrate primary combs with a sidemode-to-pump ratio as high as −2 dB, thereby leading to efficient energy conversion from the lightwave to the microwave frequency range.

OCIS codes: (060.5625) Radio frequency photonics; (140.3945) Microcavities; (190.4380) Nonlinear optics, four-wave mixing; (230.0250) Optoelectronics.

https://doi.org/10.1364/OL.42.003522

Kerr optical frequency combs aim to achieve a technologically competitive alternative for ultra-stable microwave generation [1–8]. The architecture of a Kerr comb microwave generator is conceptually very simple [9]. A whispering gallery mode (WGM) resonator with ultra-high quality factor ($Q \sim 10^9$) is first pumped by a resonant continuous-wave laser. The photon lifetime (typically >1 μs) and small mode volume enhance the nonlinear interaction of the photons via four-wave mixing in the bulk material. Therefore, a set of quasi-equidistant eigenmodes is excited, yielding an optical frequency comb in the frequency domain. Once this comb is sent to a fast photodetector, the optical carrier is retrieved, and this demodulation outputs a microwave whose frequency corresponds to the intermodal spectral spacing of the comb (and its harmonics). The advantage of this method is mainly twofold: the system is versatile in the sense that it, in principle, can output radio-frequency signals from the gigahertz to the terahertz range with the same system [10]; and the system provides both a microwave and a lightwave signal that are mutually coherent. Advanced stabilization techniques [11–14] and octave spanning [15–17] open the possibility to generate microwaves and millimeter waves with an exceptionally high degree of short- and long-term stability.

Microwave generation using Kerr optical frequency combs is effective, provided that the three following conditions are fulfilled. The first condition is that the bandwidth of the photodiode should filter out all frequencies, except one (generally, the comb intermodal frequency); this first point is merely technical, but important enough to be outlined, nevertheless. It is indeed possible to let the photodetector output multiple tones and filter them out later in the microwave domain, but these extra steps will always have a cost in terms of system simplicity and microwave purity. The second constraint is that the comb has to be highly coherent. It should ideally be free of spurious sub-harmonics, which are most of the time induced by the non-stationary amplitudes of the comb lines. Such highly coherent combs should be stationary (time-independent), and their modes have to be phase-locked. In the spatiotemporal domain, such Kerr optical frequency combs correspond to either Turing rolls or to solitons, yielding a train of quasi-equidistant pulses in the optical output port. The third and last important condition is that the sidemode-to-pump ratio of the comb should be the highest possible. Quite often, it is found both theoretically and experimentally that the output combs feature a very high intensity for the pumped (central) mode, relative to the excited sidemodes. In fact, the difference in power between the pumped modes and sidemodes is generally found to be of the order of 20 dB, or even higher. As a consequence, the photodiodes at the output port are easily saturated by the pumped mode. Whenever the comb is attenuated to avoid this photodiode saturation, the sidemodes (which are ∼100 times less powerful than the central mode) are barely above the noise floor level of the detection equipment, and feature a weak signal-to noise ratio. This results in negligible microwave output power and, accordingly, increased phase noise for the output radio-frequency signal.

Despite its critical importance, the third constraint (high sidemode-to-pump ratio) is scarcely investigated. It only starts to be explored with sufficient detail in the literature, and a first important result along that line was provided in Ref. [18], where it was shown that solitonic states could be generated with a negligible pump-to-sidemode ratio. Indeed, earlier studies have outlined that primary combs (corresponding to Turing

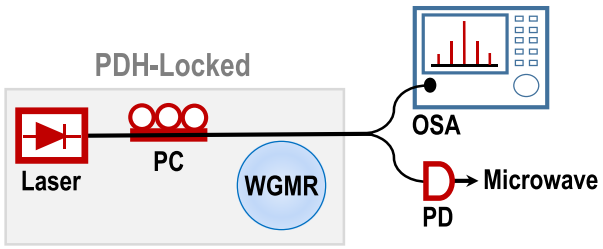

Fig. 1. Schematic illustration of the experimental setup for Kerr comb generation. PC, polarization controller; WGMR, whispering gallery mode resonator; PD, photodiode; OSA, optical spectrum analyzer; PDH, Pound–Drever–Hall.

rolls in the spatiotemporal domain) feature strong phase-locking properties [19,20] and, therefore, have a high potential for optical microwave generation [7]. In this Letter, we aim to identify the range where primary combs feature a high sidemode-to-pump ratio, thereby leading to optimal efficiency for the lightwave-to-microwave energy transfer.

The experimental setup used in this Letter is presented in Fig. 1. A tunable continuous-wave fiber laser (Koheras Adjustik) emits at a wavelength of $\lambda_L = 1550$ nm with a kilohertz linewidth. The polarization of the laser pump signal is adjusted using a fiber polarization controller, and then coupled to a magnesium fluoride (MgF_2) WGM resonator via a tapered fiber [21]. The resonator has a main radius $a = 5.7$ mm and a group velocity index $n_g = 1.37$, corresponding to a free-spectral range (FSR) equivalent to $\Omega_{\mathrm{FSR}} = c/n_g a = 2\pi \times 6.1$ GHz. The output signal from the resonator is split in two parts using an optical coupler. The first part is transmitted to a photodiode (Thorlabs InGaAs amplified PDA 10CF-EC) connected to a fast oscilloscope, where we monitor the WGM resonances. The second part is sent to a high-resolution optical spectrum analyzer (APEX 2440 B; 5 MHz resolution) which allows us to monitor the Kerr combs. The laser is stabilized to a WGM resonance with ultra-high Q factor ($\sim 10^9$) via a Pound–Drever–Hall (PDH) feedback loop.

From a theoretical point of view, the spatio-temporal dynamics of the intracavity field is generally investigated with the following Lugiato–Lefever equation (LLE) [22–24]:

$$\frac{\partial \psi}{\partial \tau} = -(1 + i\alpha)\psi + i|\psi|^2\psi - i\frac{\beta}{2}\frac{\partial^2 \psi}{\partial \theta^2} + F, \tag{1}$$

where $\psi(\theta, \tau) = \sum_l \psi_l(\tau) e^{il\theta}$ is a complex slowly varying envelope of the intracavity field, with ψ_l being the envelope of the field in the mode of reduced azimuthal order $l = \ell - \ell_0$ (note that the pump corresponds to $l = 0$, and the sidemodes symmetrically expand as $l = \pm 1, \pm 2, \ldots$). This field ψ is normalized such that $|\psi|^2$ is proportional to the number of intracavity photons. The dimensionless time τ is normalized with respect to time t as $t/2\tau_{\mathrm{ph}}$, where $\tau_{\mathrm{ph}} = Q_{\mathrm{tot}}/\omega_L$ is the photon lifetime, ω_L is the angular frequency of the pump laser, and Q_{tot} is the loaded quality factor of the WGM resonator. The angular variable $\theta \in [-\pi, \pi]$ stands for the azimuthal coordinate along the circumference of the disk-resonator. The parameter $\alpha = -2\tau_{\mathrm{ph}}(\omega_L - \omega_0)$ stands for the detuning between the laser pump and cold-resonance frequencies. The normalized parameter $\beta = 2v_g\tau_{\mathrm{ph}}\beta_2\Omega_{\mathrm{FSR}}^2$ is scaling the group-velocity dispersion (GVD) β_2 at the eigenmode frequency, and $v_g = c/n_g$ is the group velocity. We pump our resonator in the regime of anomalous GVD, for which we have $\beta < 0$. The last free parameter of the model is the pump field term F, and its square value is proportional to the laser power P following $F^2 = [8g_0\Delta\omega_{\mathrm{ext}}/\Delta\omega^3](P/\Delta\omega_0)$ where $g_0 = n_2 c\hbar\omega_0^2/n_0^2 V_0$ stands for the nonlinear gain, n_2 is the nonlinear refractive index of the material, V_0 is the effective volume of the pumped mode, and $\Delta\omega_{\mathrm{ext}}$ is the contribution of the external coupling to the resonator linewidth. The parameters are $Q_{\mathrm{in}} = 2.5 \times 10^8$ and $Q_{\mathrm{ext}} = 1.15 \times 10^9$ in our experimental setup.

Once a WGM resonance is chosen, the value of the dispersion is fixed, and different types of Kerr combs can be generated depending on the two tunable parameters of the LLE, namely the laser pump frequency α and power F^2 [21–25]. These various kinds of dissipative cavity patterns have already been extensively studied in the literature, and a comprehensive overview is provided in Ref. [9]. All stationary Kerr optical frequency combs have two important properties of particular relevance in our study: once the stationary regime is reached ($\partial\psi_l/\partial\tau \equiv 0$), symmetric sidemodes have the same intensity ($|\psi_l| = |\psi_{-l}|$), and they are phase-locked in a such a way that $\phi_l - 2\phi_0 + \phi_{-l}$ is a constant (here arbitrarily set to $2\xi_l$). However, unlike the phase sum, the phase difference $\Delta\phi_l = \phi_l - \phi_{-l}$ is not a constant of motion and depends on the initial conditions [26].

The optical signal in the output port is

$$\psi_{\mathrm{out}} = \sum_l \psi_{\mathrm{out},l} e^{il\theta}, \tag{2}$$

where $\psi_{\mathrm{out},l}$ is the modal output field in the mode l. One should note that ψ_{out} is a propagating field (and not a cavity field like ψ) and, therefore, the azimuthal angle has to be unfolded as $\theta = \Omega_{\mathrm{FSR}} t$ in Eq. (2). Hence, the output field can therefore be rewritten as

$$\psi_{\mathrm{out}}(t) = \psi_{\mathrm{out},0}\left[1 + \sum_{l>1} 2m_l e^{i\xi_l} \cos\left(l\Omega_{\mathrm{FSR}} t + \frac{1}{2}\Delta\phi_l\right)\right], \tag{3}$$

where $m_l = |\psi_{\mathrm{out},\pm l}|/|\psi_{\mathrm{out},0}|$ is the amplitude ratio between the sidemodes of order $\pm l$ and the central mode of order 0.

An infinite-bandwidth photodetector would output a radio-frequency signal proportional to the incoming optical power, which is $|\psi_{\mathrm{out}}|^2$. The generated microwave would be a multi-harmonic signal, and would feature spectral components of frequency $n \times \Omega_{\mathrm{FSR}}$, with $n = 0, 1, 2, \ldots$ The photodetected optical power can be Fourier-expanded as

$$|\psi_{\mathrm{out}}|^2 = \frac{1}{2}\mathcal{M}_0 + \sum_{n=1}^{+\infty}\left[\frac{1}{2}\mathcal{M}_n \exp(\mathrm{in}\Omega_{\mathrm{FSR}} t) + \mathrm{c.c.}\right], \tag{4}$$

where

$$\mathcal{M}_n = 2\sum_l \psi_{\mathrm{out},l+n}\psi^*_{\mathrm{out},l} \tag{5}$$

is the slowly varying envelope of the microwave spectral component of frequency $n \times \Omega_{\mathrm{FSR}}$, and c.c. stands for the complex conjugate of the preceding terms. The microwave power for the harmonic of frequency $n \times \Omega_{\mathrm{FSR}}$ can then be evaluated as $P_{\mathrm{mw},n} = \frac{1}{2}|\mathcal{M}_n|^2$, while it is equal to $P_{\mathrm{mw},0} = \frac{1}{4}|\mathcal{M}_0|^2$ for the direct current (DC) part of the microwave signal.

The above formulas are valid for all types of stationary combs, such as those induced by roll patterns, and bright or dark solitons. For the purpose of microwave generation, primary combs obtained via roll patterns are of particular interest because

they feature very strong phase-locking properties, which translate to high spectral purity, as discussed in Refs. [7,19,20]. Primary combs arise super- or sub-critically when the resonator pump F^2 is above the threshold defined as $F^2_{\text{th}} = 1 + (1-\alpha)^2$. In that case, a comb where the oscillating modes are spaced by $kL \times \Omega_{\text{FSR}}$ arises in the spectral domain (with k and L being positive integers). In the spatiotemporal domain, these primary combs yield a roll pattern characterized by L rolls in the azimuthal direction. Close to the threshold, it can be shown that $L \simeq [2(\alpha-2)/\beta]^{\frac{1}{2}}$, and this value typically increases as the system is driven far above the threshold.

Besides their strong phase-locking properties, primary combs also have another specificity that is not shared by their solitonic counterparts: the power of the oscillating modes decreases very sharply away from the pump. Therefore, it is an excellent approximation to consider only the first pair of oscillating sidemodes with eigennumbers $\pm L$, while neglecting the higher-order modes of eigennumbers $\pm kL$ with $k \geq 2$. Considering only the triplet $\{\psi_{\text{out},0}; \psi_{\text{out},L}; \psi_{\text{out},-L}\}$ in output modes implies that the generated microwave only has three spectral components as well, namely

$$\mathcal{M}_0 = 2(1+2m_L^2)|\psi_{\text{out},0}|^2, \tag{6}$$

$$\mathcal{M}_L = 4m_L e^{i\frac{\Delta\phi_L}{2}} \cos\,\xi_L |\psi_{\text{out},0}|^2, \tag{7}$$

$$\mathcal{M}_{2L} = 2m_L^2 e^{i\Delta\phi_L} |\psi_{\text{out},0}|^2. \tag{8}$$

The component $\mathcal{M}_0$ is generally the strongest and is translated by the photodetector to a DC voltage. Even though it is generally filtered out on photodetectors designed for microwave photonics applications, this component is essentially detrimental because it can eventually saturate the photodiode with no benefit in terms of microwave output power. The spectral component $\mathcal{M}_L$ corresponds to the microwave generated at the fundamental frequency $L\Omega_{\text{FSR}}$. For the purpose of microwave generation using Kerr combs, it is precisely the useful signal. The component $\mathcal{M}_{2L}$ is a second harmonic originating from the beating between the two sidemodes $\psi_{\text{out},\pm L}$: it is considered a parasitic signal, and is generally filtered out by the photodetector or by a subsequent low-pass filter.

In first approximation, it is therefore desirable to increase the modulation index m_L as much as possible, since the output microwave power of the fundamental tone $L\Omega_{\text{FSR}}$ scales as m_L^2. In that regard, the ratio m_L is a pertinent figure of merit, which can conveniently be expressed as the power difference in decibels between the first sidemodes and the pump, following $m_{L,\text{dB}} = |\psi_{\text{out},\pm L}|^2_{\text{dB}} - |\psi_{\text{out},0}|^2_{\text{dB}} = 10\,\log\,m_L^2$. Even if we consider the full primary comb, the most significant part of the microwave power will always originate from the beating between the first pair of sidemodes and the central pumped mode: this is why the best strategy to improve both the microwave power and the signal-to-noise ratio at the output of the photodetector is to tune the system in such a way that the sidemode-to-pump ratio m_L is maximal ($m_L \simeq 1$).

We have performed systematic numerical simulations in order to understand how the sidemode-to-pump ratio is modified as a function of the laser pump power and frequency. The results of these simulations are shown in Fig. 2. For various values of the detuning frequency α, the sidemode-to-pump ratio is plotted as a function of the pump power F^2. Since the generated microwave power exactly scales as $m_{L,\text{dB}}$, these curves can also be interpreted as the variations of output microwave power.

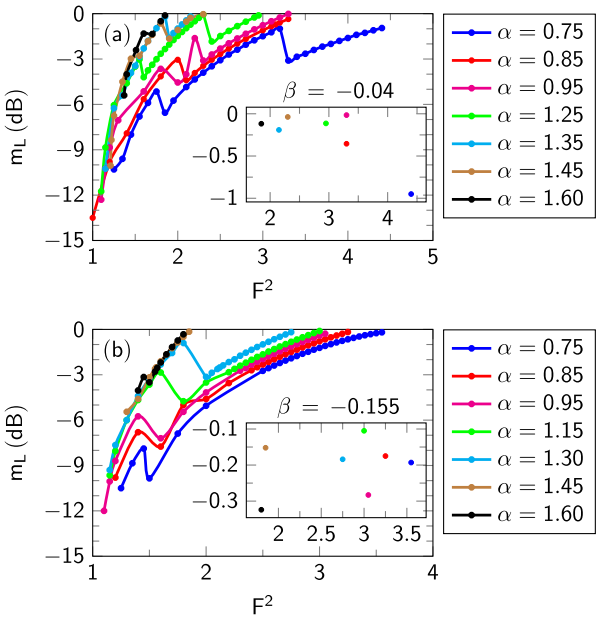

Fig. 2. Numerical simulation of the LLE for the evolution of the sidemode-to-pump ratio m_L between the pumped and the first neighboring comb line. The laser power F^2 is gradually increased for different values of the detuning α. (a) $\beta = -0.04$, and (b) $\beta = -0.155$.

It can be observed that just above to the threshold of modulational instability, this ratio is high (~12 dB). However, as the pump power is increased, this ratio converges to 0 dB, thereby indicating that $m_L \to 1$. One should note that the apparent discontinuities in these curves are induced by the jumps in the number of rolls in the Turing patterns or, equivalently, increases of the value of L.

Even though higher microwave power can be achieved by increasing m_L, a deeper analysis shows that as this modulation index is steadily increased, a larger portion of the microwave energy is wasted as well in the spectral components $\mathcal{M}_0$ and $\mathcal{M}_{2L}$. Indeed, the efficiency of the comb-to-microwave conversion at the output frequency $nL\Omega_{\text{FSR}}$ can be evaluated as $\eta_{nL} = P_{\text{mw},nL}/\sum_{k=0,1,2} P_{\text{mw},kL}$, which is the ratio between the energy of the microwave of frequency $nL\Omega_{\text{FSR}}$ and the total microwave energy. In particular, the efficiency of the conversion to the fundamental tone is explicitly defined as

$$\eta_L = \frac{8m_L^2 \cos^2 \xi_L}{(1+2m_L^2)^2 + 8m_L^2 \cos^2 \xi_L + 2m_L^4}. \tag{9}$$

The extremum condition $\partial\eta_L/\partial m_L = 0$ enables us to find that a maximal efficiency is achieved with the optimal modulation index $m_{\text{opt}} = 1/\sqrt[4]{6} \simeq 0.64$ or, equivalently, $m_{\text{opt,dB}} \simeq -3.87$ dB. Moreover, if $\cos^2 \xi_L$ is maximized to 1, η_{max} reaches an absolute maximum value $\eta_{L,\text{max}} = \frac{2}{15}\left(6-\sqrt{6}\right) \simeq 0.47$. The variations of both the microwave power and conversion efficiency are plotted in Fig. 3. It can be seen that after the peak at ≃0.64, the conversion efficiency slowly decreases while the power still increases steadily. More precisely, as m_L is increased from 0.64 to 1, the conversion efficiency only drops by 5%, while the output microwave power increases by ~250%. Figure 4 provides experimental evidence of such Kerr combs, with a sidemode-to-pump ratio around −2 dB. One can note

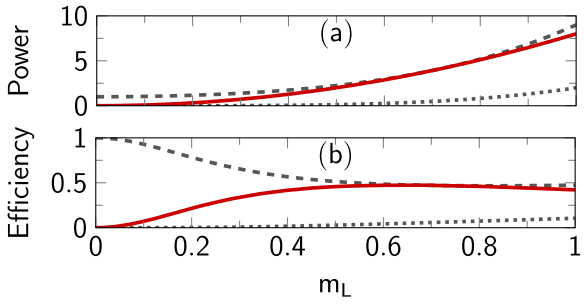

Fig. 3. Power and conversion efficiency of the microwave of frequency $L\Omega_{FSR}$ (continuous red), the DC signal of frequency 0 (dashed gray), and the second-harmonic of frequency $2L\Omega_{FSR}$ (dotted gray) as a function of the sidemode-to-pump ratio m_L. (a) Microwave power $P_{mw,nL}$ (normalized to $|\psi_{out,0}|^4$). (b) Microwave efficiency conversion η_{nL}.

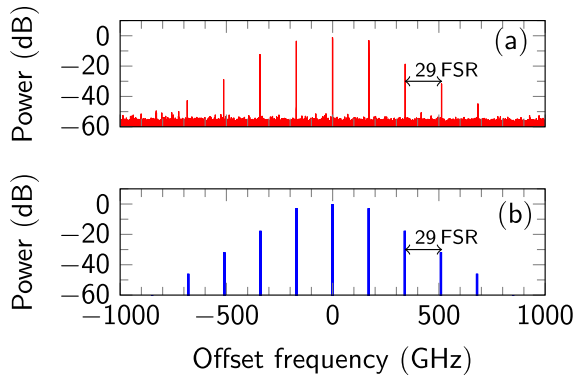

Fig. 4. Comparison between experimental and numerical primary Kerr comb spectra with $L = 29$, and featuring a sidemode-to-pump ratio of 2 dB. (a) Experimental spectrum, obtained with a laser pump power of 96 mW. (b) Numerical spectrum obtained with $\beta = -0.0048$, $\alpha = 0.78$, and $F^2 = 2.6$.

here that the intermodal frequency is relatively large (29 FSR) and falls into the millimeter wave range. However, earlier studies have shown that by pumping different families of radial modes in the same millimeter size disk-resonator permits accessing significantly different dispersion values β and, since $L \propto 1/\sqrt{\beta}$, it allows one to generate primary combs with intermodal frequencies ranging from 4 to more than 200 FSR [10].

In this Letter, we have investigated the optimization of microwave generation using primary Kerr optical frequency combs. We have shown that provided that the first pair of sidemodes is within 4 dB from the central pumped mode, more than 40% of the generated microwave energy could be transferred to the fundamental frequency. We have also experimentally evidenced such combs with a high sidemode-to-pump ratio. Future research will extend our analysis to other types of stationary combs (most notably, solitons), and we will analyze the effect of quantum [26], nonlinear [27,28], or thermodynamic fluctuations [20,29–31] on the spectral purity of the generated microwaves.

Funding. H2020 European Research Council (ERC) (278616, 632108); Centre National d'Etudes Spatiales (CNES) (SHYRO); Labex ACTION (Demo2); Region de Franche-Comte (CORPS); Universite de Franche Comte (SYOCUS).

REFERENCES

1. S. B. Papp and S. A. Diddams, Phys. Rev. A **84**, 053833 (2011).
2. J. Li, H. Lee, T. Chen, and K. J. Vahala, Phys. Rev. Lett. **109**, 233901 (2012).
3. A. A. Savchenkov, D. Eliyahu, W. Liang, V. S. Ilchenko, J. Byrd, A. B. Matsko, D. Seidel, and L. Maleki, Opt. Lett. **38**, 2636 (2013).
4. S.-W. Huang, J. Yang, J. Lim, H. Zhou, M. Yu, D.-L. Kwong, and C. W. Wong, Sci. Rep. **5**, 13355 (2015).
5. W. Liang, D. Eliyahu, V. S. Ilchenko, A. A. Savchenkov, A. B. Matsko, D. Seidel, and L. Maleki, Nat. Commun. **6**, 7957 (2015).
6. S. Arafin, A. Simsek, S.-K. Kim, W. Liang, D. Eliyahu, G. Morrison, M. Mashanovitch, A. Matsko, L. Johansson, L. Maleki, M. J. Rodwell, and L. A. Coldren, IEEE Photon. J. **9**, 6600814 (2017).
7. K. Saleh and Y. K. Chembo, Opt. Express **24**, 25043 (2016).
8. K. Saleh and Y. K. Chembo, Electron. Lett. **53**, 264 (2017).
9. Y. K. Chembo, Nanophotonics **5**, 214 (2016).
10. G. Lin and Y. K. Chembo, Opt. Express **23**, 1594 (2015).
11. P. Del'Haye, O. Arcizet, A. Schliesser, R. Holzwarth, and T. J. Kippenberg, Phys. Rev. Lett. **101**, 053903 (2008).
12. P. Del'Haye, S. B. Papp, and S. A. Diddams, Phys. Rev. Lett. **109**, 263901 (2012).
13. S. B. Papp, K. Beha, P. Del'Haye, F. Quinlan, H. Lee, K. J. Vahala, and S. A. Diddams, Optica **1**, 10 (2014).
14. P. Del'Haye, A. Coillet, T. Fortier, K. Beha, D. C. Cole, K. Y. Yang, H. Lee, K. J. Vahala, S. B. Papp, and S. A. Diddams, Nat. Photonics **10**, 516 (2016).
15. P. Del'Haye, T. Herr, E. Gavartin, M. L. Gorodetsky, R. Holzwarth, and T. J. Kippenberg, Phys. Rev. Lett. **107**, 63901 (2011).
16. Y. Okawachi, K. Saha, J. S. Levy, Y. H. Wen, M. Lipson, and A. L. Gaeta, Opt. Lett. **36**, 3398 (2011).
17. W. Liang, A. A. Savchenkov, Z. Xie, J. F. McMillan, J. Burkhart, V. S. Ilchenko, C. W. Wong, A. B. Matsko, and L. Maleki, Optica **2**, 40 (2015).
18. I. S. Grudinin, V. Huet, N. Yu, A. B. Matsko, M. L. Gorodetsky, and L. Maleki, Optica **4**, 434 (2017).
19. A. Coillet and Y. Chembo, Opt. Lett. **39**, 1529 (2014).
20. J. Pfeifle, A. Coillet, R. Henriet, K. Saleh, P. Schindler, C. Weimann, W. Freude, I. V. Balakireva, L. Larger, C. Koos, and Y. K. Chembo, Phys. Rev. Lett. **114**, 093902 (2015).
21. A. Coillet, R. Henriet, K. P. Huy, M. Jacquot, L. Furfaro, I. Balakireva, L. Larger, and Y. K. Chembo, J. Visualized Exp. e50423 (2013).
22. A. B. Matsko, A. A. Savchenkov, W. Liang, V. S. Ilchenko, D. Seidel, and L. Maleki, Opt. Lett. **36**, 2845 (2011).
23. Y. K. Chembo and C. R. Menyuk, Phys. Rev. A **87**, 053852 (2013).
24. S. Coen, H. G. Randle, T. Sylvestre, and M. Erkintalo, Opt. Lett. **38**, 37 (2013).
25. R. Henriet, G. Lin, A. Coillet, M. Jacquot, L. Furfaro, L. Larger, and Y. K. Chembo, Opt. Lett. **40**, 1567 (2015).
26. Y. K. Chembo, Phys. Rev. A **93**, 033820 (2016).
27. Y. K. Chembo, I. S. Grudinin, and N. Yu, Phys. Rev. A **92**, 43818 (2015).
28. G. Lin, S. Diallo, J. M. Dudley, and Y. K. Chembo, Opt. Express **24**, 14880 (2016).
29. S. Diallo, G. Lin, and Y. K. Chembo, Opt. Lett. **40**, 3834 (2015).
30. A. B. Matsko and L. Maleki, J. Opt. Soc. Am. B **32**, 232 (2015).
31. J. Lim, A. A. Savchenkov, E. Dale, W. Liang, D. Eliyahu, V. Ilchenko, A. B. Matsko, L. Maleki, and C. W. Wong, Nat. Commun. **8**, 8 (2017).